RESEARCH ARTICLE

Timescales of spontaneous activity fluctuations relate to structural connectivity in the brain

John Fallon[1] | **Phil Ward**[1,2] | **Linden Parkes**[1] | **Stuart Oldham**[1] | **Aurina Arnatkevičiūtė**[1] | **Alex Fornito**[1] | **Ben D. Fulcher**[3]

[1]The Turner Institute for Brain and Mental Health, School of Psychological Sciences, and Monash Biomedical Imaging, Monash University, Victoria, Australia.

[2]Australian Research Council Centre of Excellence for Integrative Brain Function, Melbourne, Australia

[3]School of Physics, The University of Sydney, NSW 2006, Australia.

Correspondence
Ben D. Fulcher, School of Physics, The University of Sydney, NSW 2006, Australia.
Email: ben.fulcher@sydney.edu.au

Funding information
AF was supported by the Sylvia and Charles Viertel Foundation. BDF was supported by an NHMRC Fellowship (1089718).

Intrinsic timescales of activity fluctuations vary hierarchically across the brain. This variation reflects a broad gradient of functional specialization in information storage and processing, with integrative association areas displaying slower timescales that are thought to reflect longer temporal processing windows. The organization of timescales across the brain is associated with cognitive function, disrupted in disease, and distinctive between individuals, but we do not yet understand how the temporal properties of activity dynamics are shaped by the brain's underlying structural-connectivity network. Using resting-state fMRI and diffusion MRI data from 100 healthy individuals from the Human Connectome Project, here we show that the timescale of spontaneous resting-state fMRI dynamics increases with the structural connectivity strength of a cortical area, matching recent results in the mouse brain. Our results hold at the level of individuals and are robust to a range of cortical parcellations. Beyond measurements of timescale, we establish a diverse BOLD dynamical signature through a comprehensive comparison to over 6000 time-series features, highlighting a wide range of interesting new temporal properties of BOLD dynamics that include measures of time-series stationarity and occurrence frequencies of symbolic

motifs. Our findings demonstrate a conserved property of mouse and human brain organization, in which a brain region's spontaneous activity fluctuations are closely related to their surrounding structural scaffold.

KEYWORDS
structure-function relationship, time-series analysis, structural connectivity, resting-state fMRI, interspecies comparison

1 | INTRODUCTION

The brain's complex spatiotemporal dynamics unfold on an intricate web of axonal connections: the connectome [1, 2]. These pathways facilitate information transfer between brain regions, manifesting in a complex relationship between connectome structure and neural dynamics. Reflecting the pairwise nature of structural connectivity (region–region), existing studies have overwhelmingly compared pairwise measurements of anatomical connectivity to pairwise statistical relationships between neural activity time series, or functional connectivity, often using simulations of network dynamics to better understand how the observed relationships may arise [3–18]. Structural connectivity is highly informative of functional connectivity, consistent with the connectome as a physical substrate constraining inter-regional communication dynamics.

Our understanding of pairwise structure–function relationships in the brain remains disconnected from our understanding of how a brain area's structural connectivity properties shape its activity dynamics. Indeed, the structural connectivity profile of a region's incoming and outgoing axonal connections is thought to define its function [19]. Furthermore, the activity dynamics of brain areas follow a functional hierarchy, with rapid dynamics in 'lower' sensory regions, and slower fluctuations in 'higher' regions associated with integrative processes [20–24]. The spatial variation of intrinsic timescales has been measured using ECOG [21], MEG [25, 26], TMS–EEG [27], and fMRI [24, 28–33], and may a function variation in temporal receptive windows: timescales over which new information can be actively integrated with recently received information [20, 33, 34]. Spatial variation in intrinsic activity fluctuations may form a key basis for the brain's functional hierarchical organization, shaped by structural variation in the brain's microcircuitry [35–37]. This organization is thought to be important for behavior and cognition [20, 38–40], and its disruption has clinical implications: e.g., differences in intrinsic timescales are associated with symptom severity in autism [33]. While much is known about the structure–function relationship at the level of brain-region pairs, and how structural and functional connectivity architecture shape cognitive function and are affected in disease [41–44], relatively little is known about how it affects the information processing dynamics of individual brain areas. In particular, we do not yet understand the role structural connections play in the cortical organization of intrinsic timescales.

Recent work has provided statistical evidence for a relationship between regional tract-tracing estimates of anatomical connectivity and rs-fMRI dynamics in the mouse brain [45]. This work took a comprehensive, data-driven approach, comparing over 7000 properties of regional BOLD dynamics (using the *hctsa* software package [46, 47]) to three key structural-connectivity properties (degree, betweenness, and clustering coefficient) measured in each of 184 brain areas. The tract-traced connectivity measurement available in mouse [48] also allowed the role of directed and weighted connectivity information to be investigated. The weighted in-degree, k_{in}^{w}, showed the strongest correlation to BOLD dynamics, particularly with its autocorrelation properties (including the Fourier spectral power in different frequency bands). For example, relative high-frequency power ($f > 0.4$ Hz) was negatively correlated to k_{in}^{w} ($\rho_V = -0.43$,

partial Spearman correlation controlling for region volume). The results suggest that structural connectivity may play a role in the spatial patterning of intrinsic timescales: brain areas with a greater aggregate strength of axonal input (highest k^w_{in}) exhibit slower timescales of spontaneous activity fluctuations, consistent with the predictions of model simulations [30, 49, 50]. Despite the low sampling rate of rs-fMRI, recent work has shown a strong correlation between timescales estimated from EEG and fMRI [33], suggesting that a similar trend may hold at much faster timescales. When ignoring edge directionality, Sethi et al. [45] found weaker but statistically significant relationships between (undirected) weighted-degree, k^w, and rs-fMRI dynamics. This suggests that a similar relationship may hold in human, where the directionality of connections cannot be measured through non-invasive MRI methods like diffusion-weighted imaging.

We know of only two investigations into how structural connectivity properties relate to BOLD dynamics in the human cortex, and both have reported weak relationships between structural connectivity strength and: (i) low-frequency rs-fMRI fluctuations, Pearson's $r = 0.12$ [32]; and (ii) the log-linear slope of the Fourier power spectrum, $r = 0.22$ [29]. These low correlations may be due to both studies measuring BOLD at a sampling rate TR $= 2.5$ s for a short duration (less than 300 volumes) in a small sample of individuals (30 [29] or 36 [32]). However, neither study controlled for region volume, which correlates strongly with the autocorrelation properties of the BOLD signal (due to the averaging of more voxelwise signals in larger areas) [45, 51]. The Human Connectome Project (HCP) dataset alleviates many of these issues, containing a large rs-fMRI dataset collected at a high sampling rate, TR $= 0.75$ s, across 1200 time points [52].

Here we characterize the rsfMRI signature of structural connectivity in the human cortex using data from the HCP [52]. In particular, we aimed to investigate whether more strongly connected regions are associated with slower timescales of BOLD activity in the human cortex, as they are in the mouse brain [45]. We report a surprisingly strong relationship, consistent with predictions from mouse: low-frequency BOLD power ($f < 0.14$ Hz) increases with structural connectivity strength, $\rho_V = 0.53$ (partial Spearman correlation correcting for region volume, $p = 2 \times 10^{-3}$). Our results hold at both the group- and individual-level, and across different cortical parcellations, reflecting a robust, interspecies conservation of how structural connectivity and regional activity dynamics are coupled in the brain.

2 | RESULTS

We investigated whether the structural connectivity strength of a cortical area is related to its spontaneous BOLD dynamics, as illustrated schematically in Fig. 1. Our methods are summarized briefly here (see Methods for details). We used data from a Human Connectome Project dataset of 100 healthy, unrelated participants (54 male, 46 female; 22–35 years old) [52]. Our main analysis focuses on the left hemisphere of the 68-region Desikan-Killiany Atlas [53] (analyses of the right hemisphere yielded similar results). Structural connectivity was estimated from the diffusion data using `MRtrix3` [54] and the FMRIB Software Library [55], performing tractography with 10 million streamlines using FACT, ACT, and SIFT-2, yielding a 34×34 left-hemisphere connectome. Following work in mouse [45], we summarized the structural connectivity of each brain area as its node strength, s, estimated as the total number of diffusion MRI-reconstructed streamlines attached to it (equivalent to weighted degree, k^w). rs-fMRI data were processed after regressing standard nuisance signals (including the global signal) and were high-pass filtered at 8×10^{-3} Hz, yielding a 34×200 (region $\times$ time) fMRI data matrix. Based on our previous findings in mouse [45], we summarized BOLD dynamics in a given brain region as the relative low-frequency power, RLFP ($f < 0.14$ Hz). Relationships between the structural properties of a cortical region and its univariate dynamics were estimated as Spearman correlation coefficients, ρ. Region volume, which varies from 49 to 4570 voxels in the Desikan-Killiany Atlas [53], is a major confound, correlating strongly with RLFP, $\rho = 0.61$ ($p = 2 \times 10^{-4}$; see Fig. S1A), as in the mouse brain [45]. To control for region volume, we

computed partial Spearman correlation coefficients, denoted here as ρ_V.

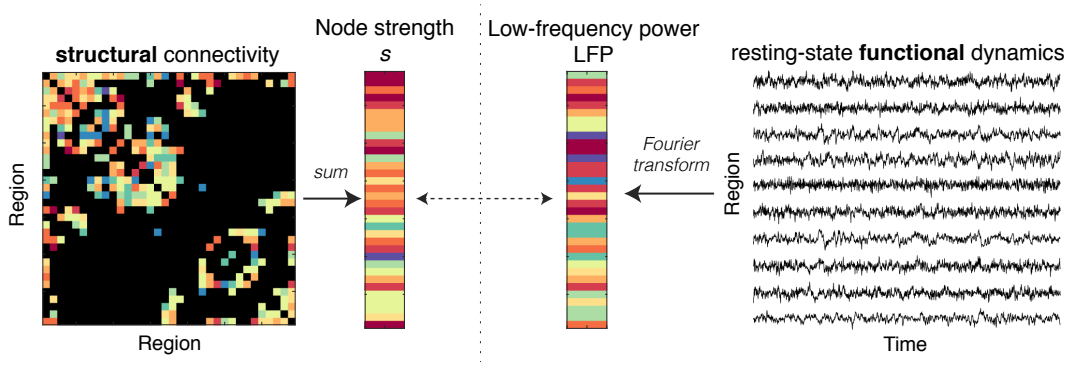

FIGURE 1 Schematic showing how we investigate the relationship between a region's structural connectivity properties to their resting-state dynamics. We summarize each cortical region as its structural connectivity strength, s, and its relative low-frequency power, RLFP ($f < 0.14$ Hz). Note that, for the purposes of schematic visualization, edge weights and node strength colors represent relative strength, from low (blue) to high (red).

2.1 | Node strength is correlated with power-spectral properties of resting-state BOLD dynamics

We first investigated the group-level relationship between connectivity strength, s, and relative low-frequency power, RLFP, by summarizing each brain region as the mean of each quantity across all 100 participants. As shown in Fig. 2A, there is a strong correlation between s and RLFP in the left hemisphere of the cortex, $\rho_V = 0.53$ (controlling for regional volume variation, $p = 2 \times 10^{-3}$). Similar results were observed in the right hemisphere $\rho_V = 0.57$ ($p = 6 \times 10^{-4}$; see Fig. S3). The positive correlation indicates that human cortical areas with greater aggregate connectivity display stronger low-frequency fluctuations, matching the relationship characterized in the mouse brain [45]. Note that RLFP is strongly correlated with region volume, $\rho = 0.61$ (Fig. S1A) and the s–RLFP relationship is stronger when region volume is not controlled for, $\rho = 0.74$ ($p < 2 \times 10^{-6}$; see Fig. S1B).

To better understand these findings, we selected three representative brain regions: the medial orbitofrontal region (low $s = 1.4 \times 10^5$), the pars triangularis (moderate $s = 4.6 \times 10^5$), and the superior parietal cortex (high $s = 1.7 \times 10^6$), as annotated in Fig. 2A. The Fourier power spectrum for each of these brain areas is plotted in Fig. 2B, with the RLFP region ($f < 0.14$ Hz) shaded. Differences in spectral power are clearest at low frequencies, especially near the peak power around 0.02 Hz. As the total power is normalized to unity, increased relative power around 0.02 Hz results in lower relative power at higher frequencies. Accordingly, the relationship with s is not sensitive to the precise RLFP frequency range ($f < 0.14$ Hz), but is reproduced with opposite sign at higher frequency bands of the same extent: $\rho_V = -0.53$ (0.14–0.28 Hz), $\rho_V = -0.56$ (0.28–0.41 Hz), $\rho_V = -0.53$ (0.41–0.55 Hz), and $\rho_V = -0.53$ (0.55–0.69 Hz).

The relationship is not dependent on parcellation. A similar relationship was found when randomly dividing each hemisphere into approximately 100 equal-sized regions [56], shown in Fig. 2C for the left hemisphere, $\rho_V = 0.53$ ($p = 1 \times 10^{-8}$). We also found a similar relationship when using the 180-region Glasser et al. [57] parcellation of the left cortex, $\rho_V = 0.43$ ($p = 3 \times 10^{-9}$; see Fig. S2), and when resampling the same number of voxels from each brain region (circumventing the need to correct for region volume variation), $\rho = 0.43$ ($p = 0.01$; see Fig. S1D). Spatial maps of both

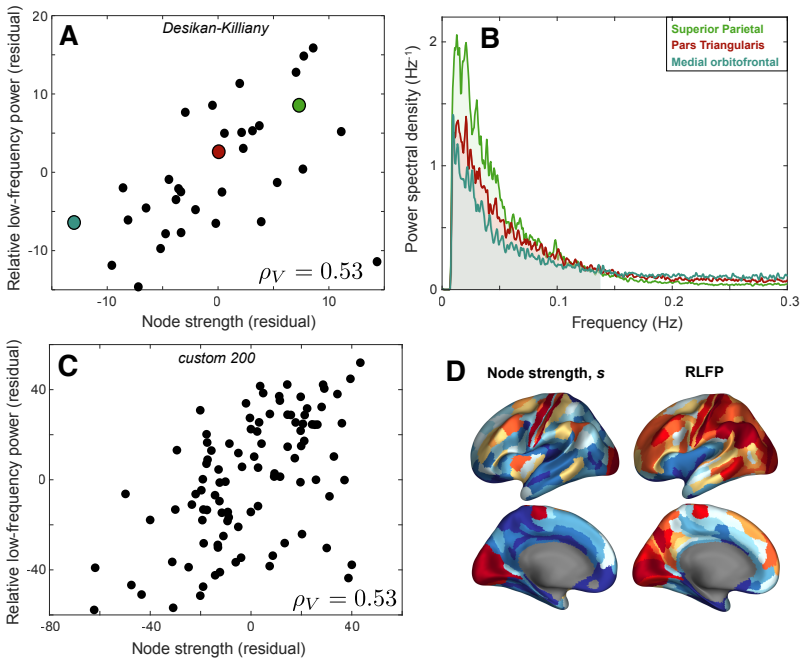

FIGURE 2 **Group-level connectivity strength, s, is positively correlated with relative low-frequency power of BOLD dynamics, RLFP ($f < 0.14$ Hz) after correcting for region volume. A**: Rank residuals of relative low-frequency power (RLFP) and node strength, s, across 34 left-hemisphere cortical regions of the Desikan-Killiany Atlas [53], after regressing out region volume. The plot reveals a positive relationship, partial Spearman's $\rho_V = 0.53$ ($p = 2 \times 10^{-3}$). **B** The group-averaged Fourier power spectra for three colored brain areas in A are plotted: medial orbitofrontal area (low s, blue), pars triangularis (moderate s, red), and superior parietal (high s, green), shown up to a maximum of 0.3 Hz. RLFP corresponds to the shaded area under the curve below 0.14 Hz. **C**: As **A**, but for 100 left-hemisphere cortical regions from a custom 200-region parcellation generated by randomly dividing each hemisphere into 100 approximately equal-sized regions [56]. **D**: Spatial maps of node strength and low-frequency power across 180 left-hemisphere cortical areas of the Glasser et al. [57] parcellation, with the relative variation of each metric shown using color, from low (blue) to high (red).

properties (at the higher spatial resolution of the Glasser et al. [57] parcellation) are shown in Fig. 2D.

2.2 | Regional structure–function relationships extend across individuals

Having demonstrated a robust group-level relationship between node connectivity strength, s, and Fourier spectral characteristics of rs-fMRI time series, we next investigated whether these results could be detected at the level of individual subjects. We measured the partial correlation coefficient, ρ_V, between s and RLFP for each individual, plotted as a distribution across all 100 individuals in Fig. 3. After false-discovery rate multiple-hypothesis correction [58], 43% of participants displayed a significant residual correlation ($p_{\text{corr}} < 0.05$: $\rho_V > 0.40$). The group-level s–RLFP relationship (annotated in Fig. 2) was stronger than the individual correlation for 91% of participants, consistent with a concentration of meaningful signal (and thus a reduction in measurement noise) through group averaging. To investigate whether inter-individual variation in s–RLFP correlation, ρ_V, is driven by in-scanner motion, we computed the Pearson

correlation between ρ_V and mean framewise displacement across individuals. We found a weak and non-significant relationship, $r = 0.10$ ($p = 0.3$), suggesting that motion is not driving our results.

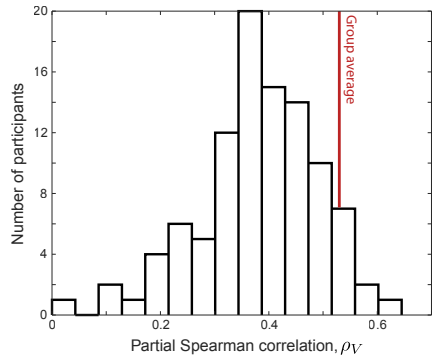

FIGURE 3 Many individuals exhibit a significant relationship between node strength, *s*, and relative low-frequency power, RLFP. The histogram of partial Spearman correlation coefficients, ρ_V, between RLFP and *s* (correcting for variations in region volume) computed separately for each of 100 individuals. The group-level result, $\rho_V = 0.54$, is shown as a vertical red line.

2.3 | Diverse properties of BOLD dynamics are informative of node strength

The results above demonstrate that Fourier spectral properties of rs-fMRI are strongly correlated with connectivity strength, *s*. But the time-series analysis literature is vast and interdisciplinary [59]; could other statistical summaries of BOLD dynamics exhibit stronger relationships to *s*? To investigated this possibility, we used the *hctsa* toolbox [46, 47] to perform a comprehensive data-driven comparison of the performance of 6062 different time-series features. The performance of each feature was measured as ρ_V (computed for each individual and then averaged across individuals). As we are interested in the magnitude of the correlation (not the sign), we took $|\rho_V|$ as the quantity of interest, plotting its distribution across all 6062 time-series features in Fig. 4. While 3768 individual time-series features exhibit a statistically significant partial correlation to *s* ($|\rho_V| > 0.39$, $p_{\text{corr}} < 0.05$), RLFP is amongst those with the highest $|\rho_V|$ (in the top 16% of all *hctsa* features). However, the distribution reveals a tail of alternative time-series features with higher $|\rho_V|$. Interestingly, these high-performing features recapitulate a familiar set of time-series features used to analyze BOLD data, as well as some unexpected new metrics. Here we summarize some notable features, labeling them by their name in *hctsa* [47]; for further descriptions of these and other features, see the Supplementary Text (Supplementary File 1 contains a full list).

Neuroimaging time series have most commonly been summarized as a measure of timescale, derived from the Fourier power spectrum or linear autocorrelation function [23, 29, 32, 33, 50]. Our highly comparative time-series analysis highlights many features measuring similar temporal properties. One example is `SP_Summaries_fft_linfitloglog_mf_a2`, $\rho_V = -0.59$, which estimates the powerlaw exponent of the Fourier power spectrum (as a linear fit in a log-log plot, fitted after excluding the lower and upper quarter of frequencies), reminiscent of Hurst exponent estimation from neural time series [60]. Another interesting high-performing feature is an information-theoretic analogue of the first zero-crossing of the autocorrelation function: the first minimum of the automutual information function [61, 62] computed after differencing the time series: `IN_AutoMutualInfoStats_diff_20_kraskov1_4_fmmi`, $\rho_V = -0.63$. This incremental dif-

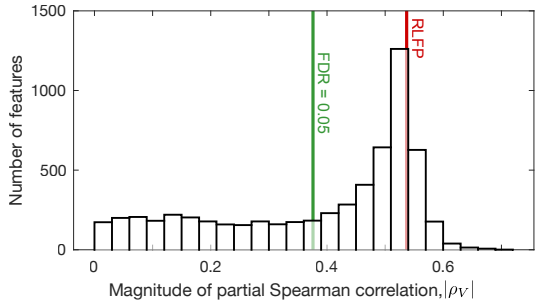

FIGURE 4 RLFP has amongst the strongest correlations to connectivity strength, *s*, in a comparison to 6062 time-series features. We plot a histogram of absolute partial Spearman correlation coefficients, $|\rho_V|$, between each of 6062 rs-fMRI time-series features and connectivity strength *s* (controlling for region volume). The features were computed using the *hctsa* toolbox [46, 47]. RLFP ($|\rho_V| = 0.53$) is shown red, and the 5% FDR-corrected statistical-significance threshold ($|\rho_V| > 0.39$) is shown green.

ferencing step, a common time-series transformation used to stabilize the mean [63], also emerged in a range of symbolic motif features. Symbolic motifs count the frequency of a particular set of consecutive symbols in a time series that has been converted to a symbolic string using a simple coding rule, e.g., coding stepwise increases as 'U' (up) and decreases as 'D' (down). Motifs associated with small movements are consistent with slow fluctuations and showed positive correlations with *s* (e.g., the 'AABB' pattern: `SB_MotifThree_diffquant_aabb`, $\rho_V = 0.62$), whereas motifs associated with rapid changes exhibited strong negative correlations (e.g., the 'up-down-up-up' pattern: `SB_MotifTwo_diff_uduu`, $\rho_V = -0.62$). The symbolization process may help to capture informative signal in noisy rs-fMRI time series, with symbolic motifs emerging as a simple yet powerful new tool to analyze neuroimaging signals.

Increased rs-fMRI recording durations have allowed dynamic functional connectivity analyses to characterize changes in functional connectivity across the timescale of the recording [64]. Our data-driven analysis highlighted a range of univariate analogues of this concept, flagging a range of high-performing features measuring time-series stationarity. For example, `SY_SlidingWindow_sampen_ent10_2`, $\rho_V = -0.65$, measures how local estimates of the entropy metric, SampEn$(2, 0.1)$ [65], vary across the time series. *hctsa* also highlighted novel features derived from visibility graphs, which represent each fMRI time point as a node and constructing network edges using visibility rules [66, 67]. For example, *s* is highly correlated to a simple outlier metric of the visibility graph degree distribution, `NW_VisibilityGraph_norm_ol90`, $\rho_V = 0.66$.

Our results demonstrate the usefulness of *hctsa* in determining the most useful time-series analysis methods for a given problem in an automated, data-driven manner. By interpreting the features, *hctsa* provides new understanding of how rs-fMRI dynamics relate to structural connectivity strength, flagging an ensemble of time-series features that both encapsulate conventional approaches to analyzing BOLD dynamics, and introduces novel ones.

3 | DISCUSSION

In this work, we demonstrate that the variation of intrinsic fMRI timescales across human cortical areas is related to the variation of structural connectivity strength, matching a regional structure–function relationship previously observed the mouse brain. This strong interspecies consistency is despite major differences in measurement between mouse (axonal tract tracing and rs-fMRI in 18 anesthetized mice) and human (DWI and rs-fMRI in 100 awake participants).

In both species, brain areas with a greater aggregate strength of axonal connectivity exhibit slower rs-fMRI BOLD fluctuations, consistent with a hierarchical gradient of intrinsic timescales [20–23]. Our results are robust to cortical parcellation, hold at the level of individuals, and are not driven by motion. We also introduce a highly comparative time-series analysis approach to the problem which, in a completely data-driven way, recapitulates conventional BOLD signal analysis approaches and highlights a range of promising new temporal features for characterizing neuroimaging data. This study expands the investigation of the brain's structure–function relationship to the level of individual regions (rather than pairs of regions), providing a more complete picture of how the brain's intricate axonal scaffold shapes spontaneous brain dynamics. Continuing investigations of the structure–function relationship at the level of individual areas will allow us to better understand how the brain's local circuits shape its dynamics and relate these results to hypotheses about the principles governing the brain's spatiotemporal organization.

Our results demonstrate that areas that are more strongly connected to the rest of the brain (and thus candidates for areas with more integrative function) have slower average timescales. This relationship is consistent with a hierarchy of timescales in which more highly connected areas (high in the hierarchy) serve a more integrative function, integrating diverse information over longer timescales than the fast dynamics and behavioral responses associated with lower sensory areas [21–24, 45, 49, 50]. While many previous studies have reported interareal variation in intrinsic timescales [21, 24, 26, 28–31, 33], to our knowledge, only two prior human studies have related this variation to structural connectivity [29, 32]. Both studies found weak relationships, $r = 0.12$ [32] and $r = 0.22$ [29], using hand-picked dynamical properties of rs-fMRI time series in small sample sizes, and without correcting for variations in regional volume. The much stronger correlation reported here, $\rho_V = 0.53$ (after correcting for region volume), may be due to the high-quality imaging data (1200 volumes at a sampling period of 0.75 s) in a larger sample of 100 individuals. Although the low temporal resolution of fMRI is a major limitation of studying neural activity timescales, recent work has indicated a significant and strong correlation between timescales estimated from simultaneously recorded EEG and fMRI (γ band, adjusted $r^2 = 0.71$) [33], suggesting that our results may reflect characteristic differences at faster timescales. Future multimodal research could probe intrinsic processing timescales to provide a more complete temporal picture of how timescales are structured across the cortex in different species, and its implications for cognition and disease.

While fMRI is most frequently characterized in terms of pairwise correlations (functional connectivity), our results highlight the utility of characterizing local brain dynamics. BOLD dynamics are distinctive to individuals [25], play a role in cognitive function [20], and are disrupted in disease [33]. They also play a role in brain organization, being related to the functional and structural connections of an area, and may provide an indirect measure of its information-processing capabilities [28, 29]. Generating summaries of activity dynamics at individual brain areas also yields spatial maps that can be related to other datasets, such as macroscale maps of microstructural variation [36, 68] straightforwardly. While univariate analysis of the BOLD signal is promising, a common problem in analyzing univariate time series is selecting an appropriate analysis method or summary statistic to compute [59]. The neuroimaging literature has most commonly focused on linear autocorrelation properties, either measured directly from the autocorrelation function or via the Fourier power spectrum. *hctsa* circumvents the need for subjectivity or manual exploration across a vast time-series analysis literature [47], providing a data-driven means of selecting the most relevant types of time-series features for a given problem. By comparing the behavior of thousands of diverse time-series analysis methods [47], *hctsa* finds meaningful and interpretable temporal features that best characterize structural connectivity strength, *s*: recapitulating conventional timescale-based metrics, and also flagging a range of novel features related to symbolic motifs, stationarity, and visibility graphs. The common theme of applying incremental differencing, a transformation commonly used to stabilize the mean [63], suggests that applying this transformation to BOLD data could enhance the informative signal that can be extracted from it. We also note the prominent performance of time-series stationarity properties, suggesting a fruitful avenue in further characterizing this property, which may loosely be considered a univariate analogue of

dynamical functional connectivity [64]. We expect that *hctsa* will be especially useful in discovering informative time-series features from data streams with higher sampling rates than fMRI, such as those measured using ECoG, MEG, and EEG. Future work should pay particular care to the data-processing pipeline, which can substantially affect results obtained from modalities including fMRI [69]. Because quality metrics are typically assessed on the basis of functional connectivity, the extent to which preprocessing steps affect the univariate properties of fMRI data is less well understood.

Understanding how time-series properties vary across cortical areas also has important practical implications for how functional connectivity is estimated and interpreted. We first draw attention to the strong variation of time-series properties with region volume (i.e., as more voxel-wise time series are averaged into a region-level time series), and the strong conservation of this relationship between mouse and human [45]. This confound of parcellation is not typically acknowledged or addressed, but is crucial to account for in future work by performing partial correlations using region volume as a regressor and/or using a parcellation containing regions of equal volume. Variations in properties like autocorrelation also affect how significance testing can be accurately applied to functional-connectivity data [51, 70].

This study highlights the ability of direct interspecies comparisons to accumulate evidence for common properties of brain organization. Organizational properties that are shared across scales and species [71] are strong candidates for being under evolutionary selection pressures for serving an important functional advantage. These range from the properties of networks abstracted from the brain's physical structure—like rich club connectivity and modularity—through to hierarchical gradients [35, 36] and the patterning of gene expression with structural connectivity [72–74]. The current study adds a regional relationship between structure and function to this set of conserved relationships; future work is needed to establish whether a similar pattern holds across other species, such as *C. elegans* and non-human primates [75], where both structural connectivity and large-scale brain dynamics have been measured.

Our findings suggest that the brain exploits a range of timescales to efficiently store, process, and transfer information, with these timescales coupled to the underlying structural connectivity properties of a brain area [28] in the same way in the mouse brain and human cortex. The results are strengthened by their consistency across species and scales, and are consistent with interareal connectivity playing a direct causal role in shaping intrinsic timescales, as recent computational models have hinted at [30, 49]. However, our results are also consistent with gradients of cortical microstructure driving differences in spontaneous dynamics [18, 26], with interareal connectivity simply varying along this gradient. In the absence of experiments that can legion or manipulate structural connectivity, computational modeling will play a crucial role in providing mechanistic explanations of the statistical relationships characterized here, towards a causal understanding of the mechanisms through which intrinsic timescales are shaped. Given the cognitive importance of how timescales are organized across the cortex [31, 33], understanding the physical mechanisms shaping BOLD dynamics could lead to novel new treatments that aim to rectify abnormal timescales in the brain, e.g., using a transcranial magnetic stimulation (TMS) protocol [40] tailored to an individual's structural-connectivity profile. Integrating data across species and scales to elucidate common relationships, and using theoretical modeling approaches to propose possible mechanisms underlying those patterns, will be key to understanding how the brain's organization allows it to efficiently process and integrate information.

4 | DATA AND METHODS

All code for reproducing our analyses is at `https://github.com/johnfallon/humanStructureFunction`. The data that support the findings of this study are available from the Human Connectome Project (HCP) at `https://db.humanconnectome.org`.

4.1 | Data acquisition and preprocessing

MRI data were downloaded from the Human Connectome Project (HCP) [52]. We selected the HCP 100 unrelated participants dataset (54 males, 46 females) for detailed analysis [52], as in previous work [76]. All participants were healthy and aged between 22–35 years and provided written informed consent; ethics was approved by the Institutional Review Board of Washington University. We used the minimally preprocessed data of which full details can be found elsewhere [77]; a broad overview is provided here.

4.1.1 | Diffusion-weighted imaging

A 3T Siemens Skyra scanner with a customized head coil (100 mT/m maximum gradient strength and a 32 channel head coil) located at Washington University, St Louis, was used to acquire all neuroimaging data.

Diffusion data were acquired using a spin-echo EPI sequence with the following parameters: TR/TE = 5520/89.5 ms, slice thickness = 1.25 mm, 111 slices, 1.25 mm isotropic voxels. Three gradient shells of 90 diffusion-weighted directions and six b0 images were collected with right-to-left and left-to-right phase encoding polarities for each of the three diffusion weightings (1000, 2000, and 3000 s/mm^2). For additional imaging parameters see Glasser et al. [77]. The diffusion data had been pre-processed using the HCP diffusion pipeline [77], which included normalization of b0 image intensity across runs, correction for EPI susceptibility and eddy-current-induced distortions, gradient-nonlinearities, subject motion and application of a brain mask.

Subsequent processing of the diffusion data used `MRtrix3` [54] and FMRIB Software Library [55]. Tractography was conducted using Fibre Assignment by Continuous Tracking (FACT), a deterministic measure [78, 79] This deterministic measure was selected over probabilistic methods because it is less prone to false-positive connections [80], which have been shown to be more detrimental to network construction than false negative connections [81]. A total of 10 million streamlines were generated with a step size of 0.125 mm. Streamlines terminated when the curvature exceed 45°, when the fractional anisotropy value was less than 0.1, or if the length was greater than 250 mm.

In order to further improve the biological accuracy of the structural networks, Anatomically Constrained Tractography (ACT) and Spherically Informed Filtering of Tractograms (SIFT-2) were applied alongside and to the tractography data. ACT delineates the brain into different tissue types (e.g., cortical grey matter, subcortical grey matter, white matter, CSF). This information is then used while tractography is being conducted to ensure streamlines are beginning, traversing, and terminating in anatomically correct locations [82]. Another issue hampering tractography is the density of reconstructed connections is not reflective of the underlying diffusion data [83]. SIFT-2 addresses this limitation by modeling the expected density of connections as calculated from the diffusion signal before comparing this prediction to the connection densities obtained in tractography. Streamlines are then weighted by a cross-sectional area multiplier determined by this model fit [84]. This same model of diffusion density was also used to dynamically choose streamline seeding points during tractography [84].

Our main cortical parcellation was the 68-region Desikan–Killiany Atlas [53] (34 regions per hemisphere). To demonstrate robustness of our results, we also compared two additional parcellations: (i) Glasser et al.'s 360-region HCP parcellation (180 regions per hemisphere) [57], and (ii) a custom built 200-node parcellation (100 regions per hemisphere) which was formed by randomly dividing each hemisphere into 100 approximately equal-sized cortical regions [56]. These parcellations were generated on the Freesurfer-extracted surfaces for each subject and then projected to volumetric space.

As in the mouse [45], we focused our analysis on a single hemisphere. Analyzing ipsilateral connectivity also has the advantage of avoiding errors associated with reconstructing long-range contralateral connections using diffusion

tractography [Reveley et al., 2015]. Ipsilateral structural connectivity within the left hemisphere was represented as a weighted, undirected 34×34 adjacency matrix, A_{ij}, where each entry captures the number of streamlines with termination points within 5 mm of either regions i and j. A group-weighted structural connectome, G_{ij}, was constructed by retaining inter-regional connections that were present in more than 75% of participants [85], and setting edge weights to the average value across participants (where zero entries were not included in the average). The resulting adjacency matrix had an edge density of 25%, and edge weights varying from 322 to 7.6×10^4. Following Sethi et al. [45], each brain region was summarized as its connectivity strength, s, calculated by summing all streamlines connected to a region (after applying ACT and SIFT-2).

4.1.2 | Resting-state fMRI

Resting-state fMRI (rs-fMRI) data were downloaded from the HCP database [52]. Images were obtained using a gradient-echo, echo planar image (EPI) sequence with the following parameters: TR/TE = 720/33.1 ms, slice thickness = 2.0 mm, 72 slices, 2.0 mm isotropic voxels, frames per run = 1200. We used the volumetric EPI data from the first rs-fMRI session (left-right phase encoding), processed and denoised using ICA-FIX [86].

Subsequent processing of the rs-fMRI data was performed. First, the rs-fMRI time series were linearly detrended. Then, to provide more stringent control over nuisance signals we regressed the rs-fMRI data against mean white matter (WM) and mean cerebrospinal fluid (CSF) as well as the global signal (GS) using `fsl_regfilt`. Specifically, grey matter (GM), WM, and CSF probability masks were generated using SPM8's New Segment routine. The WM and CSF masks were thresholded and binarized, retaining only voxels with $> 99\%$ probability. The GM mask was thresholded and binarized to retain only voxels with $> 50\%$ probability. The binary GM mask was then subtracted from the binary WM and CSF masks to ensure no gray matter voxels were present in the estimation of the WM and CSF nuisance signals. Estimating the GS was done by taking the union of two whole brain masks created using FSL's `bet` function applied to the spatially normalized EPI and T1-weighted images [69]. All nuisance time series were extracted by taking the mean over all voxels in the respective masks. Finally, we removed low-frequency fluctuations using a high-pass filter with a hard threshold of 8×10^{-3} Hz, applied to the EPI data via a fast Fourier transform. Once processed, EPI time series were summarized at the level of brain regions by averaging voxel time series over all voxels within each parcel.

4.2 | BOLD time-series analysis

For each brain region (34 left-hemisphere regions for our default parcellation) in each subject, we extracted a BOLD time series. Following Sethi et al. [45], we focused our main analysis on the power across frequency bands of the discrete Fourier transform of each BOLD time series. BOLD time series were linearly detrended and normalized to unit variance using a z-score before applying a fast Fourier transform. Variance normalization ensures that the total power in the Fourier power spectrum is unity; the power in a given frequency band represents relative power and is unitless. In this work, we refer to relative low-frequency power (RLFP) as the proportion of power contained in the lowest 20% of frequencies ($f < 0.14$ Hz), as in Sethi et al. [45].

To investigate how the performance frequency-band power properties compares to alternative univariate time-series properties, we compared across a comprehensive sample of time-series features [46] implemented as the *hctsa* toolbox (v0.96) [47], available at `https://github.com/benfulcher/hctsa`. This software was used to extract over 7000 features from each rs-fMRI time series. Following standard procedures [47], we filtered features that returned special values (features inappropriate for these data) or were approximately constant across all brain regions (features provide no meaningful information). We then restricted our analysis to 6062 well-behaved features that were not

filtered from any participant.

To investigate the dependence of our results to variations in region volume [45], we estimated the volume of each region in our parcellation by summing the number of 0.7 mm isotropic voxels in a region using the T1-weighted image. Region volume was controlled for by computing a partial Spearman correlation. We used Spearman rank correlations due to the frequently non-normally distributed nodal properties, particularly region volume and node strength.

ACKNOWLEDGEMENTS

We would like to thank Leonardo Gollo and Dan Lurie for thoughtful and helpful comments on the manuscript.

REFERENCES

[1] Fornito A, Zalesky A, Bullmore E. Fundamentals of brain network analysis. Academic Press; 2016.

[2] Sporns O, Tononi G, Kötter R. The Human Connectome: A Structural Description of the Human Brain. PLoS Comp Biol 2005 Sep;1(4):e42.

[3] Abdelnour F, Voss HU, Raj A. Network diffusion accurately models the relationship between structural and functional brain connectivity networks. NeuroImage 2014 Apr;90:335–347.

[4] Abdelnour F, Dayan M, Devinsky O, Thesen T, Raj A. Functional brain connectivity is predictable from anatomic network's Laplacian eigen-structure. NeuroImage 2018;172:728–739.

[5] Deco G, Jirsa VK. Ongoing Cortical Activity at Rest: Criticality, Multistability, and Ghost Attractors. J Neurosci 2012 Mar;32(10):3366–3375.

[6] Deco G, Ponce-Alvarez A, Mantini D, Romani GL, Hagmann P, Corbetta M. Resting-state functional connectivity emerges from structurally and dynamically shaped slow linear fluctuations. J Neurosci 2013 Jul;33(27):11239–11252.

[7] Deco G, McIntosh AR, Shen K, Hutchison RM, Menon RS, Everling S, et al. Identification of optimal structural connectivity using functional connectivity and neural modeling. J Neurosci 2014 Jun;34(23):7910–7916.

[8] Finger H, Bönstrup M, Cheng B, Messé A, Hilgetag CC, Thomalla G, et al. Modeling of Large-Scale Functional Brain Networks Based on Structural Connectivity from DTI: Comparison with EEG Derived Phase Coupling Networks and Evaluation of Alternative Methods along the Modeling Path. PLoS Comp Biol 2016 Aug;12(8):e1005025.

[9] Ghosh A, Rho Y, McIntosh AR, Kötter R, Jirsa VK. Noise during Rest Enables the Exploration of the Brain's Dynamic Repertoire. PLoS Comp Biol 2008 Oct;4(10):e1000196.

[10] Goñi J, van den Heuvel MP, Avena-Koenigsberger A, de Mendizabal NV, Betzel RF, Griffa A, et al. Resting-brain functional connectivity predicted by analytic measures of network communication. Proc Natl Acad Sci USA 2014;111(2):833–838.

[11] Hagmann P, Cammoun L, Gigandet X, Meuli R, Honey CJ, Wedeen VJ, et al. Mapping the Structural Core of Human Cerebral Cortex. PLoS Biol 2008 Jul;6(7):e159.

[12] Hermundstad AM, Bassett DS, Brown KS, Aminoff EM, Clewett D, Freeman S, et al. Structural foundations of resting-state and task-based functional connectivity in the human brain. Proceedings of the National Academy of Sciences 2013;110(15):6169–6174.

[13] Van Den Heuvel MP, Mandl RC, Kahn RS, Hulshoff Pol HE. Functionally linked resting-state networks reflect the underlying structural connectivity architecture of the human brain. Human brain mapping 2009;30(10):3127–3141.

[14] Honey CJ, Kötter R, Breakspear MJ, Sporns O. Network structure of cerebral cortex shapes functional connectivity on multiple time scales. Proc Natl Acad Sci USA 2007 Jun;104(24):10240–10245.

[15] Honey CJ, Sporns O, Cammoun L, Gigandet X, Thiran JP, Meuli R, et al. Predicting human resting-state functional connectivity from structural connectivity. Proc Natl Acad Sci USA 2009 Feb;106(6):2035–2040.

[16] Mišić B, Betzel RF, de Reus MA, van den Heuvel MP, Berman MG, McIntosh AR, et al. Network-Level Structure-Function Relationships in Human Neocortex. Cereb Cortex 2016 Jun;26(7):3285–3296.

[17] Skudlarski P, Jagannathan K, Calhoun VD. Measuring brain connectivity: diffusion tensor imaging validates resting state temporal correlations. NeuroImage 2008;.

[18] Wang P, Kong R, Kong X, Liégeois R, Orban C, Deco G, et al. Inversion of a large-scale circuit model reveals a cortical hierarchy in the dynamic resting human brain. Science Advances 2019 Jan;5(1):eaat7854.

[19] Passingham RE, Stephan KE, Kötter R. The anatomical basis of functional localization in the cortex. Nat Rev Neurosci 2002 Aug;3(8):606–616.

[20] Hasson U, Chen J, Honey CJ. Hierarchical process memory: memory as an integral component of information processing. Trends in Cognitive Sciences 2015 Jun;19(6):304–313.

[21] Honey CJ, Thesen T, Donner TH, Silbert LJ, Carlson CE, Devinsky O, et al. Slow Cortical Dynamics and the Accumulation of Information over Long Timescales. Neuron 2012 Oct;76(2):423–434.

[22] Kiebel SJ, Daunizeau J, Friston KJ. A Hierarchy of Time-Scales and the Brain. PLoS Comp Biol 2008 Nov;4(11):e1000209.

[23] Murray JD, Bernacchia A, Freedman DJ, Romo R, Wallis JD, Cai X, et al. A hierarchy of intrinsic timescales across primate cortex. Nat Neurosci 2014 Dec;17(12):1661–1663.

[24] Stephens GJ, Honey CJ, Hasson U. A place for time: the spatiotemporal structure of neural dynamics during natural audition. J Neurophysiol 2013 Nov;110(9):2019–2026.

[25] Keitel A, Gross J. Individual Human Brain Areas Can Be Identified from Their Characteristic Spectral Activation Fingerprints. PLoS Biol 2016 Jun;14(6):e1002498.

[26] Demirtas M, Burt JB, Helmer M, Ji JL, Adkinson BD, Glasser MF, et al. Hierarchical Heterogeneity across Human Cortex Shapes Large-Scale Neural Dynamics. Neuron 2019 Feb;0(0):1181–1194.e13.

[27] Rosanova M, Casali A, Bellina V, Resta F, Mariotti M, Massimini M. Natural frequencies of human corticothalamic circuits. J Neurosci 2009 Jun;29(24):7679–7685.

[28] Baria AT, Baliki MN, Parrish T, Apkarian AV. Anatomical and Functional Assemblies of Brain BOLD Oscillations. J Neurosci 2011 May;31(21):7910–7919.

[29] Baria AT, Mansour A, Huang L, Baliki MN, Cecchi GA, Mesulam MM, et al. Linking human brain local activity fluctuations to structural and functional network architectures. NeuroImage 2013 Jun;73(C):144–155.

[30] Cocchi L, Sale MV, Gollo LL, Bell PT, Nguyen VT, Zalesky A, et al. A hierarchy of timescales explains distinct effects of local inhibition of primary visual cortex and frontal eye fields. eLife 2016 Sep;5:e15252.

[31] Huang Z, Liu X, Mashour GA, Hudetz AG. Timescales of Intrinsic BOLD Signal Dynamics and Functional Connectivity in Pharmacologic and Neuropathologic States of Unconsciousness. J Neurosci 2018 Feb;38(9):2304–2317.

[32] Lee TW, Xue SW. Linking graph features of anatomical architecture to regional brain activity: A multi-modal MRI study. Neuroscience Letters 2017 Jun;651:123–127.

[33] Watanabe T, Rees G, Masuda N. Atypical intrinsic neural timescale in autism. eLife 2019 Feb;8:839.

[34] Hasson U, Yang E, Vallines I, Heeger DJ, Rubin N. A Hierarchy of Temporal Receptive Windows in Human Cortex. J Neurosci 2008 Mar;28(10):2539–2550.

[35] Burt JB, Demirtas M, Eckner WJ, Navejar NM, Ji JL, Martin WJ, et al. Hierarchy of transcriptomic specialization across human cortex captured by structural neuroimaging topography. Nat Neurosci 2018 Aug;27:889.

[36] Fulcher BD, Murray JD, Zerbi V, Wang XJ. Multimodal gradients across mouse cortex. Proc Natl Acad Sci USA 2019 Feb;116(10):4689–4695.

[37] García-Cabezas MÁ, Joyce MKP, John YJ, Zikopoulos B, Barbas H. Mirror trends of plasticity and stability indicators in primate prefrontal cortex. Eur J Neurosci 2017 Oct;46(8):2392–2405.

[38] Cavanagh SE, Wallis JD, Kennerley SW, Hunt LT. Autocorrelation structure at rest predicts value correlates of single neurons during reward-guided choice. eLife 2016 Oct;5:1096.

[39] Runyan CA, Piasini E, Panzeri S, Harvey CD. Distinct timescales of population coding across cortex. Nat Neurosci 2017;.

[40] Gollo LL. Computational Psychiatry: Exploring atypical timescales in the brain. eLife 2019 Feb;8:e15252.

[41] Li Y, Liu Y, Li J, Qin W, Li K, Yu C, et al. Brain anatomical network and intelligence. PLoS computational biology 2009;5(5):e1000395.

[42] Penke L, Maniega SM, Bastin M, Hernández MV, Murray C, Royle N, et al. Brain white matter tract integrity as a neural foundation for general intelligence. Molecular psychiatry 2012;17(10):1026.

[43] Fornito A, Zalesky A, Breakspear MJ. The connectomics of brain disorders. Nat Rev Neurosci 2015 Mar;16(3):159–172.

[44] van den Heuvel MP, Sporns O. A cross-disorder connectome landscape of brain dysconnectivity. Nat Rev Neurosci 2019 May;1:1.

[45] Sethi SS, Zerbi V, Wenderoth N, Fornito A, Fulcher BD. Structural connectome topology relates to regional BOLD signal dynamics in the mouse brain. Chaos 2017 Apr;27(4):047405.

[46] Fulcher BD, Little MA, Jones NS. Highly comparative time-series analysis: the empirical structure of time series and their methods. J Roy Soc Interface 2013 Jun;10(83):20130048–20130048.

[47] Fulcher BD, Jones NS. *hctsa*: A Computational Framework for Automated Time-Series Phenotyping Using Massive Feature Extraction. Cell Sys 2017 Nov;5(5):527–531.e3.

[48] Oh SW, Harris JA, Ng L, Winslow B, Cain N, Mihalas S, et al. A mesoscale connectome of the mouse brain. Nature 2014 Apr;508(7495):207–214.

[49] Gollo LL, Zalesky A, Hutchison RM, van den Heuvel MP, Breakspear MJ. Dwelling quietly in the rich club: brain network determinants of slow cortical fluctuations. Phil Trans Roy Soc B 2015 May;370(1668):20140165–20140165.

[50] Chaudhuri R, Knoblauch K, Gariel MA, Kennedy H, Wang XJ. A Large-Scale Circuit Mechanism for Hierarchical Dynamical Processing in the Primate Cortex. Neuron 2015 Oct;88(2):419–431.

[51] Afyouni S, Smith SM, Nichols TE. Effective Degrees of Freedom of the Pearson's Correlation Coefficient under Serial Correlation. bioRxiv 2018;p. 453795.

[52] Van Essen DC, Smith SM, Barch DM, Behrens TEJ, Yacoub E, Ugurbil K. The WU-Minn Human Connectome Project: An overview. NeuroImage 2013 Oct;80:62–79.

[53] Desikan RS, Ségonne F, Fischl B, Quinn BT, Dickerson BC, Blacker D, et al. An automated labeling system for subdividing the human cerebral cortex on MRI scans into gyral based regions of interest. Neuroimage 2006;31(3):968–980.

[54] Tournier JD, Calamante F, Connelly A. MRtrix: diffusion tractography in crossing fiber regions. International journal of imaging systems and technology 2012;22(1):53–66.

[55] Jenkinson M, Beckmann CF, Behrens TE, Woolrich MW, Smith SM. Fsl. Neuroimage 2012;62(2):782–790.

[56] Fornito A, Zalesky A, Bassett DS, Meunier D, Ellison-Wright I, Yücel M, et al. Genetic influences on cost-efficient organization of human cortical functional networks. J Neurosci 2011 Mar;31(9):3261–3270.

[57] Glasser MF, Coalson TS, Robinson EC, Hacker CD, Harwell J, Yacoub E, et al. A multi-modal parcellation of human cerebral cortex. Nature 2016 Jul;536(7615):171–178.

[58] Benjamini Y, Hochberg Y. Controlling the False Discovery Rate: A Practical and Powerful Approach to Multiple Testing. J Roy Stat Soc B 1995;57(1):289–300.

[59] Fulcher BD. Feature-Based Time-Series Analysis. In: Feature Engineering for Machine Learning and Data Analytics CRC Press; 2018.p. 87–116.

[60] He BJ. Scale-Free Properties of the Functional Magnetic Resonance Imaging Signal during Rest and Task. J Neurosci 2011 Sep;31(39):13786–13795.

[61] Kantz H, Schreiber T. Nonlinear time series analysis, vol. 7. Cambridge university press; 2004.

[62] Lizier JT. JIDT: An Information-Theoretic Toolkit for Studying the Dynamics of Complex Systems. Front Robot AI 2014 Dec;1:1085.

[63] Hyndman RJ, Athanasopoulos G. Forecasting: principles and practice. OTexts; 2018.

[64] Hutchison RM, Womelsdorf T, Allen EA, Bandettini PA, Calhoun VD, Corbetta M, et al. Dynamic functional connectivity: promise, issues, and interpretations. Neuroimage 2013;80:360–378.

[65] Richman JS, Moorman JR. Physiological time-series analysis using approximate entropy and sample entropy. American Journal of Physiology-Heart and Circulatory Physiology 2000 Jun;278(6):H2039–H2049.

[66] Lacasa L, Luque B, Ballesteros F, Luque J, Nuño JC. From time series to complex networks: The visibility graph. Proc Natl Acad Sci USA 2008 Apr;105(13):4972–4975.

[67] Sannino S, Stramaglia S, Lacasa L, Marinazzo D. Visibility graphs for fMRI data: Multiplex temporal graphs and their modulations across resting-state networks. Network Neuroscience 2017 May;2015:1–14.

[68] Huntenburg JM, Bazin PL, Bazin PL, Margulies DS. Large-Scale Gradients in Human Cortical Organization. TICS 2017;22(1):21–31.

[69] Parkes L, Fulcher BD, Yücel M, Fornito A. An evaluation of the efficacy, reliability, and sensitivity of motion correction strategies for resting-state functional MRI. NeuroImage 2018 May;171:415–436.

[70] James O, Park H, Kim SG. Impact of sampling rate on statistical significance for single subject fMRI connectivity analysis. Hum Brain Map 2019 Apr;5(3):537.

[71] van den Heuvel MP, Bullmore ET, Sporns O. Comparative Connectomics. Trends in Cognitive Sciences 2016 Mar;20(5):345–361.

[72] Fulcher BD, Fornito A. A transcriptional signature of hub connectivity in the mouse connectome. Proc Natl Acad Sci USA 2016 Feb;113(5):1435–1440.

[73] Arnatkeviciūtė A, Fulcher BD, Pocock R, Fornito A. Hub connectivity, neuronal diversity, and gene expression in the Caenorhabditis elegans connectome. PLoS Comp Biol 2018 Dec;14(2):e1005989.

[74] Fornito A, Arnatkeviciūtė A, Fulcher BD. Bridging the Gap between Connectome and Transcriptome. Trends in Cognitive Sciences 2019 Nov;23(1):34–50.

[75] Shen K, Bezgin G, Everling S, McIntosh AR. A macaque connectome for large-scale network simulations in TheVirtualBrain. bioRxiv 2018;https://www.biorxiv.org/content/early/2018/11/28/480905.

[76] Parkes L, Fulcher BD, Yücel M, Fornito A. Transcriptional signatures of connectomic subregions of the human striatum. Genes, Brain and Behavior 2017 May;25(7):1176–663.

[77] Glasser MF, Sotiropoulos SN, Wilson JA, Coalson TS, Fischl B, Andersson JL, et al. The minimal preprocessing pipelines for the Human Connectome Project. NeuroImage 2013 Oct;80:105–124.

[78] Mori S, Crain BJ, Chacko VP, Van Zijl PC. Three-dimensional tracking of axonal projections in the brain by magnetic resonance imaging. Annals of Neurology: Official Journal of the American Neurological Association and the Child Neurology Society 1999;45(2):265–269.

[79] Mori S, Van Zijl PC. Fiber tracking: principles and strategies–a technical review. NMR in Biomedicine: An International Journal Devoted to the Development and Application of Magnetic Resonance In Vivo 2002;15(7-8):468–480.

[80] Thomas C, Frank QY, Irfanoglu MO, Modi P, Saleem KS, Leopold DA, et al. Anatomical accuracy of brain connections derived from diffusion MRI tractography is inherently limited. Proceedings of the National Academy of Sciences 2014;111(46):16574–16579.

[81] Zalesky A, Fornito A, Cocchi L, Gollo LL, van den Heuvel MP, Breakspear M. Connectome sensitivity or specificity: which is more important? Neuroimage 2016;142:407–420.

[82] Smith RE, Tournier JD, Calamante F, Connelly A. Anatomically-constrained tractography: improved diffusion MRI streamlines tractography through effective use of anatomical information. Neuroimage 2012;62(3):1924–1938.

[83] Smith RE, Tournier JD, Calamante F, Connelly A. SIFT: spherical-deconvolution informed filtering of tractograms. Neuroimage 2013;67:298–312.

[84] Smith RE, Tournier JD, Calamante F, Connelly A. SIFT2: Enabling dense quantitative assessment of brain white matter connectivity using streamlines tractography. Neuroimage 2015;119:338–351.

[85] van den Heuvel MP, Sporns O. Rich-club organization of the human connectome. J Neurosci 2011 Nov;31(44):15775–15786.

[86] Smith SM, Beckmann CF, Andersson J, Auerbach EJ, Bijsterbosch J, Douaud G, et al. Resting-state fMRI in the human connectome project. Neuroimage 2013;80:144–168.